Dynamic stability analysis of a standalone photovoltaic microgrid on a dynamic load in a rural area

Cyriaque Bosco Mitokpè
Department of Electrical Engineering
Polytechnic School of Abomey-Calavi (EPAC)
Abomey-Calavi, Benin
boscomitokpe@gmail.com

François-Xavier Nicolas Fifatin
Department of Electrical Engineering
Polytechnic School of Abomey-Calavi (EPAC)
Abomey-Calavi, Benin
fifatinf@gmail.com

Richard Gilles Agbokpanzo
Department of ENSET-Lokossa
National University of Science, Technology, Engineering and Mathematics of Abomey (UNSTIM)
Abomey, Benin
richgille@gmail.com

Amevi Acakpovi
Department of Electrical/Electronic Engineering
Accra Technical University
Accra, Ghana
acakpovia@gmail.com

Audace B. K. Didavi
Department of Electrical Engineering
Polytechnic School of Abomey-Calavi (EPAC)
Abomey-Calavi, Benin
didavia@gmail.com

2022 International Conference on Green Energy, Computing and Sustainable Technology (GECOST) | 978-1-6654-8663-7/22/$31.00 ©2022 IEEE | DOI: 10.1109/GECOST55694.2022.10010389

***Abstract*— This paper analyzes the dynamic stability of the voltage amplitude of a photovoltaic generator feeding a dynamic load. We focused on a photovoltaic field with an output of about 20 kWp, a three-phase PWM-controlled voltage inverter and 7.5 kW three-phase induction motor (IM) driving a load for rural use. MATLAB / SIMULINK is used for the simulations. The results of the simulation on a resistive load and on a dynamic load which is the three-phase induction motor with a load torque of 40 N.m showed that the relative voltage drop is more than 12% in the transient regime and about 3% in steady state. This variation shows the instability of the system's voltage amplitude due to lack of inertia. It is therefore essential in these types of microgrids to improve the dynamic stability of the voltage amplitude for an effective and efficient use. To do this, a first solution to this voltage instability is to hybridize the solar photovoltaic system with an inertial voltage source which is the wind source.**

Keywords*— *dynamic amplitude stability, photovoltaic generator, dynamic load, isolated microgrid, wind source.

I. INTRODUCTION

In the Republic of Benin, the national electrification rate in 2020 is 30.4%, including 5.7% in rural areas, and the national electricity access rate is 33.42%, including 8.78% in rural areas. The rate of access to electricity better reflects the reality on the ground, it has an average increase of only 0.78% between 2016 and 2020 [1].

To this end, it is therefore necessary to build microgrids based on several decentralized renewable generators (Photovoltaic Generator; Wind Generator, Biomass and others) to cope not only with the increase in energy demand of rural populations but also for towns far from conventional electricity grid.

Thus, many microgrids based on photovoltaic generator have been built throughout the country by the Government and by private companies [2]. Photovoltaic technology has been one of the most promising renewable energies due to its ability to generate electricity without any environmental pollution [3].

However, due to the very random and discontinuous nature of the solar photovoltaic energy source, the combination of several renewable energy sources to make a hybrid system connected to the electrical grid or isolated, is becoming increasingly common [4], [5].

The quality of electrical energy has become a major concern for both consumers and electric power suppliers. So, maintaining the frequency deviations and the voltage amplitude within their predefined range becomes critical in standalone grid [6].

For this purpose, many voltage stability studies (amplitude and/or frequency) on hybrid systems have been done with different methods and conditions. For example, the authors of references [7], [8] have shown that the voltage instability comes from the power electronic devices used for the different conversions. Those of the references [6], [9], [10] have suspected the load.

Given all this, it seemed interesting to study the dynamic behavior of the voltage amplitude of an isolated photovoltaic generator feeding a dynamic load which is a three-phase induction motor and a linear load which is a resistive load for comparison. We used Matlab/simulink for the simulations.

II. SYSTEM'S COMPONENTS MODELING

This paper shows a dynamic stability analysis of an isolated photovoltaic microgrid on a dynamic load in a rural area. The system consists of photovoltaic solar panels, a three-phase voltage inverter and the dynamic load is made of a three-phase asynchronous motor driving a grain mill. The model of each component of the system is implemented and simulated in Matlab/Simulink.

A. Photovoltaic solar panels modeling

PV celles are modelled using one diode or two diodes equivalent circuit. For this work, we choose one diode model as shown in Fig. 1. The PV current can be determined as shown in (1) to (4) [3].

The mathematical equations that describes the current-voltage (I-V) characteristics of ideal photovoltaic cell as follows.

$$I = I_{pv} - I_d \quad (1)$$

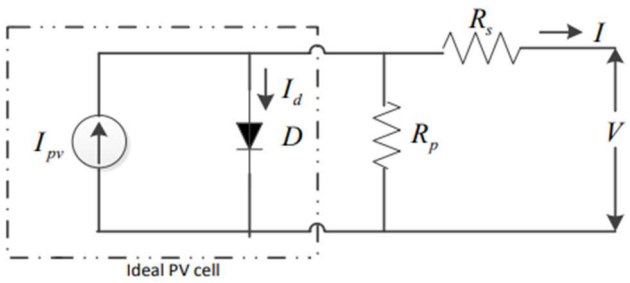

Fig. 1. Equivalent circuit of Solar cell [3].

where I is the net current which makes a difference of photo current I_{pv} and diode current I_d. R_p is the shunt or parallel resistance which is neglected and R_s is PV cell series resistance. I_d and I_{pv} are defined as:

$$I_d = I_s\left[exp\left(\frac{q\cdot(V+I\cdot R_s)}{A\cdot K\cdot T_c}\right)-1\right] \quad (2)$$

$$I = I_{pv} - I_s\left[exp\left(\frac{q\cdot(V+I\cdot R_s)}{A\cdot K\cdot T_c}\right)-1\right] \quad (3)$$

where,

I_s is the diode saturation current;

q is the electric charge;

K is the Boltzmann's constant;

T_c is the cell temperature;

R_p is the PV cell parallel resistance;

A is the ideality factor.

To get additive voltage and higher amperage, we connect some PV modules in series and some in parallel [11].

The terminal equation for current of a PV module becomes as follows:

$$I = N_p\cdot\left[I_{ph} - I_s\left[exp\left(\frac{q\cdot\left(\frac{V}{N_s}+\frac{I\cdot R_s}{N_p}\right)}{A\cdot K\cdot T_c}\right)-1\right] - \frac{\left(\frac{V}{N_s}+\frac{I\cdot R_s}{N_p}\right)}{R_p}\right] \quad (4)$$

where,

N_s is the PV module serie cells number;

N_p is the PV module parallel cells number.

The above given equation is for single diode model, where ideal factor A is equal to one. If two diode model is used then this factor ranges between 1 to 2. Generally, optimization technique is used to determine a suitable value for a model. This parameter plays a vital role in a Photovoltaic cell.

B. Modeling of DC-AC converter with his control

The three-phase voltage inverter electric circuit is shown in Fig. 2 and its is represented by the relation:

$$\begin{bmatrix}V_a\\V_b\\V_c\end{bmatrix} = \frac{V_{DC}}{3}\begin{bmatrix}2&-1&-1\\-1&2&-1\\-1&-1&2\end{bmatrix}\begin{bmatrix}C_a\\C_b\\C_c\end{bmatrix} \quad (5)$$

The output voltages (V_a, V_b and V_c) of the inverter are a function of the logic controls (C_a, C_b and C_c) of the arms which constitute it and of the input voltage V_{DC} as shown in (5).

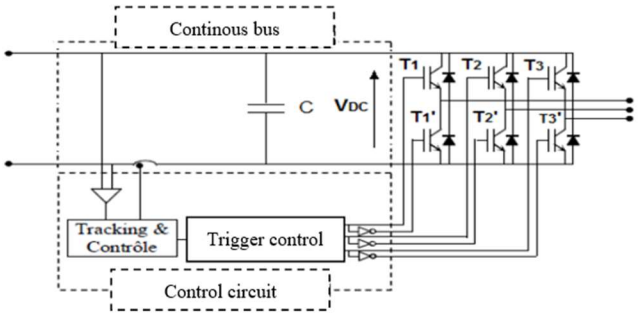

Fig. 2. Electric circuit of the three-phase voltage inverter [12].

The implementation of this inverter control is done in Matlab/Simulink.

C. Modeling of three-phase Induction Motor

As the 3-phase IM is widely used in industries because of robust construction, good speed regulation and high-power factor [4], [10] we choose to use it as the dynamic load connected to the PV sources.

The dynamic model of the system will be done by taking into account the transient and steady state of the induction motor. Simplification assumptions are made for the simulation purposes [12].

1) General electrical equations of the three-phase Induction Motor: The three-phase electrical equations of the motor in matrix form are presented in (6) to (9).
Equations (6) and (7) are those relating to the voltages of the motor stator and rotor respectively [12].

$$[v_{sabc}] = [R_s][i_{sabc}] + \frac{d}{dt}[\varphi_{sabc}] \quad (6)$$

$$[v_{rabc}] = [R_r][i_{rabc}] + \frac{d}{dt}[\varphi_{rabc}] \quad (7)$$

where,

$[R_s]$ et $[R_r]$ are respectively the resistances matrix of the stator and of the rotor by phase;

$[v_{sabc}]$, $[v_{rabc}]$, $[i_{sabc}]$et $[i_{rabc}]$ are respectively the voltage and current matrix of the stator and of the rotor.

The flux are expressed as a function of the currents by involving the various inductances in (8) and (9) such as:

$$[\varphi_{sabc}] = [L_s][i_{sabc}] + [M_{sr}][i_{rabc}] \quad (8)$$

$$[\varphi_{rabc}] = [M_{sr}][i_{sabc}] + [L_r][i_{rabc}] \quad (9)$$

where,

$[\varphi_{sabc}]$ et $[\varphi_{rabc}]$ are the stator and rotor flux matrix;

$[L_s]$ et $[L_r]$ are stator and rotor inductances matrix respectively;

$[M_{sr}]$ is the mutual inductance matrix between a phase of the stator and a phase of the rotor.

2) Mechanical equations of the Induction Motor: The operation mechanical equations of the asynchronous motor can be put in the form:

$$J\frac{d\Omega}{dt} = C_{em} - f_v\Omega - C_r \qquad (10)$$

where,

J represents the inertia moment of the machine under study;

Ω is the motor rotational speed;

C_{em} is the machine electromagnetic torque;

f_v is the motor viscous friction;

C_r is the motor load torque.

For reasons of simplicity, we use the transformation of Park to express the three-phase equations of the IM in a rotating two-phase frame (d-q). This transformation ensures the invariance of the instantaneous power between the three-phase markers (120°) and the two-phase mark (90°). Then, considering the nonlinearity of the motor, and choosing the axis d coincident with the axis of the rotor (reference related to the rotor: $\omega_r = 0$ and $\omega_s = \omega = P\Omega$). The dynamic mathematical model of the IM in the rotating frame d-q become [13]:

$$\begin{bmatrix} v_{sd} \\ v_{sq} \\ 0 \\ 0 \end{bmatrix} = \begin{bmatrix} R_s & -\omega_s l_s & 0 & -\omega_s L_m \\ \omega_s l_s & R_s & \omega_s L_m & 0 \\ -R_r & 0 & R_r & 0 \\ 0 & -R_r & 0 & R_r \end{bmatrix} \begin{bmatrix} i_{sd} \\ i_{sq} \\ i_{md} \\ i_{mq} \end{bmatrix} + \begin{bmatrix} l_s & 0 & L_{md} & L_{dq} \\ 0 & l_s & L_{dq} & L_{mq} \\ -l_r & 0 & l_r + L_{md} & L_{dq} \\ 0 & -l_r & L_{dq} & l_r + L_{mq} \end{bmatrix} \begin{bmatrix} \frac{di_{sd}}{dt} \\ \frac{di_{sq}}{dt} \\ \frac{di_{md}}{dt} \\ \frac{di_{mq}}{dt} \end{bmatrix} \qquad (11)$$

The mechanical equation of the motor will then become:

$$J\frac{d\Omega}{dt} = PL_m\left(i_{md}i_{sq} - i_{mq}i_{sd}\right) - f_v\Omega - C_r \qquad (12)$$

where: $\Omega = \frac{d\theta}{dt}$

The implementation of all of the above equations in Matlab/Simulink is presented in Fig. 3. The essential characteristics of PV module and IM are presented in TABLES I and II respectively.

TABLE I. PV MODULE CHARACTERISTICS [15]

Parameters	Values
Power at STC (W)	240
Vmp: Voltage at Max Power (V)	30.72
Imp: Current at Max Power (A)	7.83
Voc: Open Circuit Voltage (V)	36.84
Isc: Short Circuit Current (A)	8.32
Nominal Operating Cell Temp (°C)	46.4

TABLE II. INDUCTION MOTOR NOMINAL TECHNICAL CHARACTERISTICS

Parameters	Values
Power (kW) / (HP)	7.5 / 10
Supply voltage 3~(V)	230/400
Current intensity (A)	14.6
Rotation speed (rpm)	1440 – 4 poles
Frequency (Hz)	50-60

III. RESULTS AND DISCUSSION

To make our analysis, we first simulated the behavior of the photovoltaic generator facing a linear load (resistive load). Secondly, we add the three-phase induction motor without any torque load. Finally, we analyse the voltage fluctuations of the PV generator supplying power to three phase motor which drives a 40 N.m load. We have arranged the two types of loads in parallel whose operation is controlled by switches K1 (resistor control) and K2 (IM control).

First, we simulated the behavior of the voltages at the output of the solar array (PV) and at the output of the voltage inverter in front of a linear load (resistive load). Thus, we closed the switch of the resistors K1 at 0.2 second while the one K2 of the IM is open. The results are shown in Fig. 4.

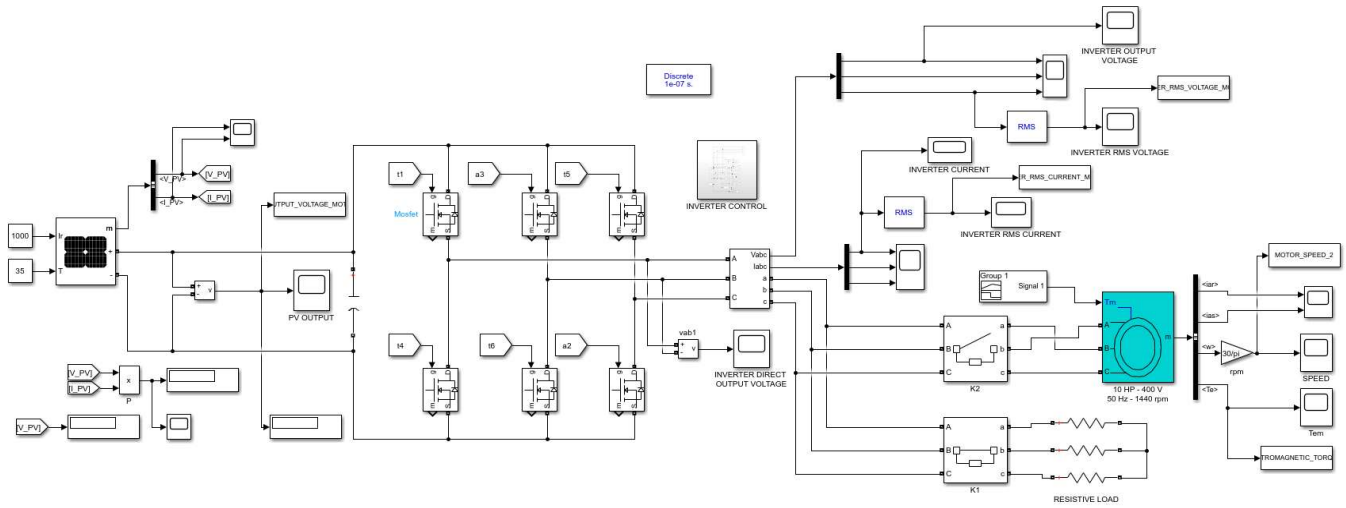

Fig. 3. Simulink block diagram of the network model

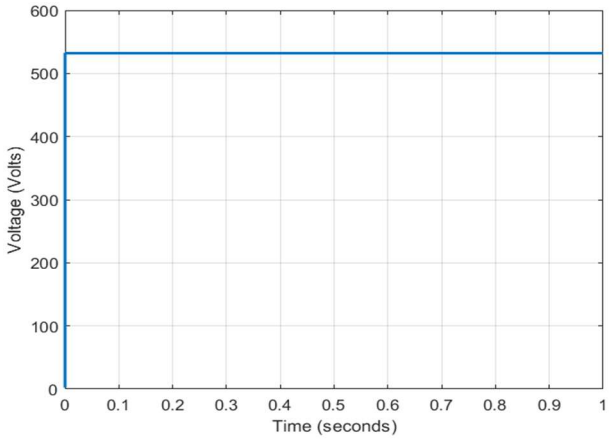

Fig. 4. PV output voltage with linear load

We observed in the Fig. 4 a slight constant variation of the value of the PV output voltage with linear load. It is the same thing with the inverter RMS output voltage with linear load.

In a second step, we simulated the system with the three-phase motor which runs freely. To do this, K1 remained open during the whole simulation time. To be sure that the IM starts, we closed K2 at 0.2 seconds. The behavior of the output voltage of the PV plant is shown in Fig. 5 and Fig. 6.

These figures show respectively the zoom of the voltage when the motor is in transient and steady state. The transient regime ranges from about 0.2 seconds to 0.36 seconds.

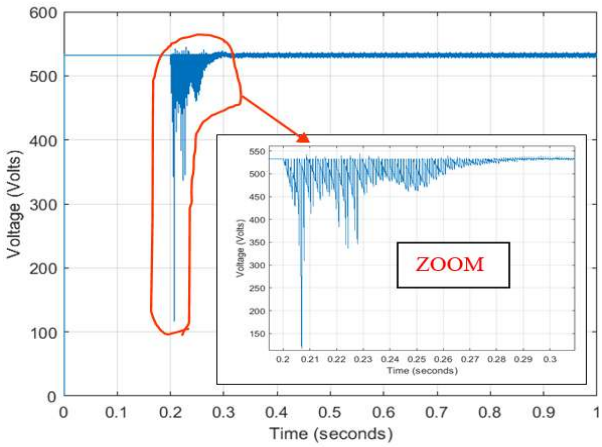

Fig. 5. PV output voltage with unloaded IM (Zoom of transient regime)

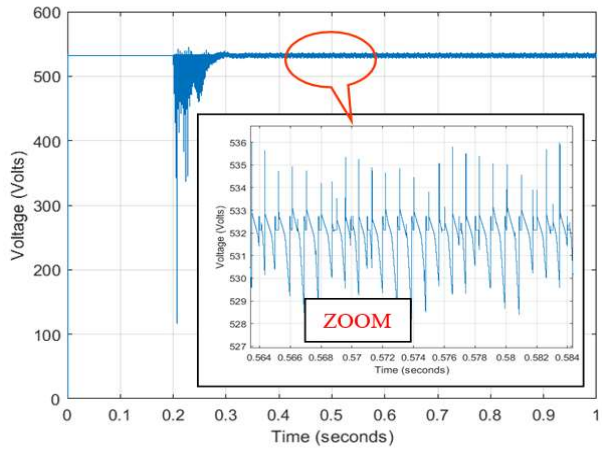

Fig. 6. PV output voltage with unloaded IM (Zoom of steady state)

We notice that the voltage is strongly perturbed. The voltage at no load of 532.12 Volts passes abruptly to 117.32 Volts that is to say a relative variation of more than nearly 78% in the transient regime. It oscillates between 535.97 Volts and 528.69 Volts in the steady state.

Fig.7 shows the behavior of the RMS value of the output voltage of the three-phase inverter that supplies the motor. In the transient regime, the RMS value of the voltage goes from 395.26 Volts (at no load) to 346.78 Volts, i.e. a relative drop in voltage of more than 12% before returning to 394.71 Volts to stabilize at 394.66 Volts.

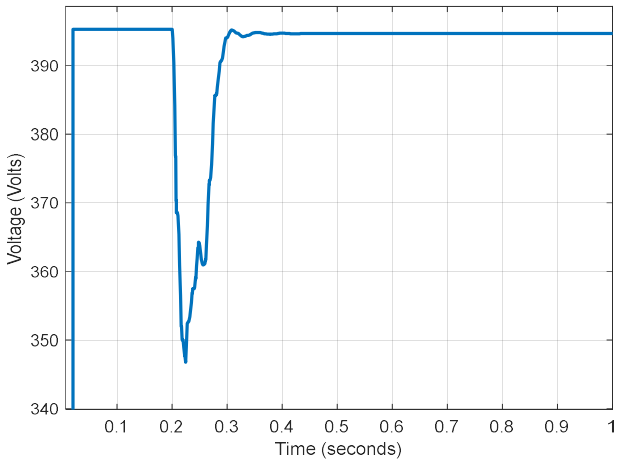

Fig. 7. Inverter RMS output voltage with motor only at no load

Finally, we simulated the system on the dynamic load (IM) by applying a load torque of 40 N.m. K1 always remained open during the whole simulation time. We closed K2 at 0.2 seconds and applied the load torque at 0.5 seconds and cancelled it at 0.8 seconds. The behaviors of the PV array output voltage and inverter RMS output voltage signal are shown in Fig. 8 and Fig. 9 respectively.

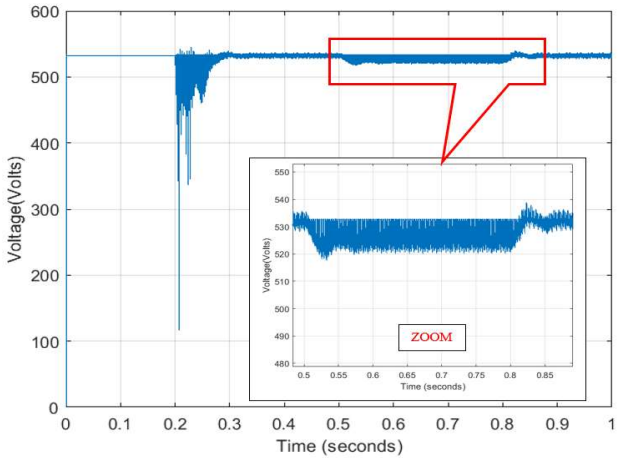

Fig. 8. PV output voltage with IM under load

In Fig. 8, we observe an almost constant voltage drop during the whole time the load remained connected. The Fig. 9 shows that if the load is applied to the motor, the voltage decreases from 394.66 Volts to 386.00 Volts, i.e. a relative variation of almost 3%.

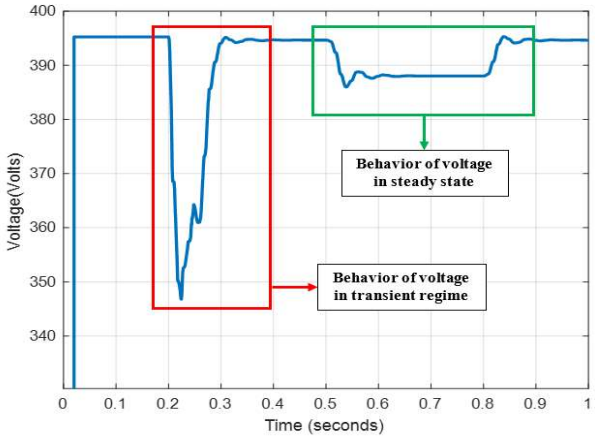

Fig. 9. Inverter RMS output voltage with IM under load

The behavior of the RMS value of the current when the IM under load is connected is shown in Fig. 10. It shows that in the transient regime from 0.2 seconds to about 0.36 seconds, the current value rises sharply from 0 to 70.87 Amperes before stabilizing at 5.45 Amperes in the steady state (with unloaded IM). When we connect the load at 0.5 seconds, we observe a small peak of 16.56 Amperes. The stabilization is obtained at 13.65 Amperes.

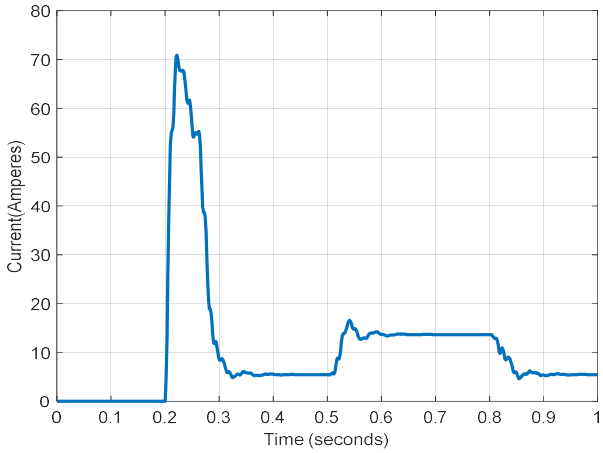

Fig. 10. Inverter RMS current with IM under load

IV. CONCLUSION

Simulation results of the studied microgrid show a relative voltage drop that varies from 3% to over 12% the inverter RMS output voltage. Those results prove that the voltage amplitude of the photovoltaic generator is seriously affected when supplying power to dynamic load like induction motors. This may be caused by the harmonic power drawn by the dynamic load connection and also to other parameters. Consequently, the improvement of dynamic voltage stability is essential in standalone microgrids.

To do so, we would correct this voltage instability by exploring solutions such as adding an inertial source to the photovoltaic source, or studying harmonic distortion by identifying the specific harmonic order involved and applying suitable mitigation methods to alleviate the Total Harmonic Distortion (THD) problem.

REFERENCES

[1] Direction Générale des Ressources Énergétiques (Bénin), "Chiffres clés 2021 Bilans énergétiques et indicateurs 2016 à 2020," Cotonou, Bénin, 2021. Accessed: Sep. 28, 2021. [Online]. Available: https://direction-energie.gouv.bj/telecharger-chiffres-cles

[2] "Plan directeur d'électrification hors-réseau : fiche de synthèse - Publications - Millennium Challenge Account Bénin II." https://mcabenin2.bj/media/publication/show/null/1/plan-directeur-delectrification-hors-reseau-fiche-de-synthese (accessed Aug. 30, 2022).

[3] G. Jain, A. S. V.K, and U. S, "Modelling and simulation of solar photovoltaic fed induction motor for water pumping application using perturb and observer MPPT algorithm," in *2016 International Conference on Energy Efficient Technologies for Sustainability (ICEETS)*, Apr. 2016, pp. 250–254. doi: 10.1109/ICEETS.2016.7582935.

[4] K. Poncelet, H. Höschle, E. Delarue, A. Virag, and W. D'haeseleer, "Selecting Representative Days for Capturing the Implications of Integrating Intermittent Renewables in Generation Expansion Planning Problems," *IEEE Transactions on Power Systems*, vol. 32, no. 3, pp. 1936–1948, May 2017, doi: 10.1109/TPWRS.2016.2596803.

[5] B. Ming, P. Liu, L. Cheng, Y. Zhou, and X. Wang, "Optimal daily generation scheduling of large hydro–photovoltaic hybrid power plants," *Energy Conversion and Management*, vol. 171, pp. 528–540, Sep. 2018, doi: 10.1016/j.enconman.2018.06.001.

[6] Q. L. Lam, "Advanced control of microgrids for frequency and voltage stability: robust control co-design and real-time validation," phdthesis, Université Grenoble Alpes, 2018. Accessed: Nov. 17, 2021. [Online]. Available: https://tel.archives-ouvertes.fr/tel-01836292

[7] A. Houari, "Contribution à l'étude de micro-réseaux autonomes alimentés par des sources photovoltaïques," phdthesis, Université de Lorraine, 2012. Accessed: Mar. 02, 2022. [Online]. Available: https://hal.univ-lorraine.fr/tel-01749469

[8] A. Choudhury, S. Mohanty, S. Pati, A. B. Nanda, A. K. Naik, and S. K. Kar, "Voltage and Frequency Stabilization of a Hybrid Autonomous System Using SMC-Based STATCOM Equipped with BESS," in *Advances in Electrical Control and Signal Systems*, Singapore, 2020, pp. 959–967. doi: 10.1007/978-981-15-5262-5_74.

[9] L. Lin, X. Zhao, J. Zhu, X. Zhang, and R. Yang, "Simulation Analysis of Microgrid Voltage Stability with Multi-induction Motor Loads," *Electric Power Components and Systems*, vol. 46, no. 5, pp. 560–569, Mar. 2018, doi: 10.1080/15325008.2018.1459958.

[10] A. Loubna, T. Riad, and M. Salima, "Standalone photovoltaic array fed induction motor driven water pumping system," *International Journal of Electrical and Computer Engineering*, vol. 10, no. 5, p. 4534, 2020.

[11] M. Catelani, L. Ciani, L. Cristaldi, M. Faifer, M. Lazzaroni, and M. Rossi, "Characterization of photovoltaic panels: The effects of dust," in *2012 IEEE International Energy Conference and Exhibition (ENERGYCON)*, Sep. 2012, pp. 45–50. doi: 10.1109/EnergyCon.2012.6348198.

[12] S. Nemsi, L. Barazane, S. Diaf, and A. Malek, "Comparative study between two maximum power point tracking (MPPT) techniques for photovoltaic system," *Journal of Renewable Energies*, vol. 16, no. 4, Art. no. 4, Dec. 2013.

[13] A. G. Hounkpe-Houenou, "Commande prédictive par facts de la régulation de la tension et de la fréquence d'une génératrice asynchrone auto excitée," UAC, Abomey-Calavi, 2017.

[14] K. Idjdarene, "Contribution à l'étude et la commande de génératrices asynchrones à cage dédiées à des centrales électriques éoliennes autonomes," These de doctorat, Lille 1, 2010. Accessed: Nov. 17, 2021. [Online]. Available: http://www.theses.fr/2010LIL10124

[15] "SolarHub - PV Module Details: A10J-M60-240 - by A10Green Technology." http://www.solarhub.com/product-catalog/pv-modules/3320-A10J-M60-240-A10Green-Technology (accessed Sep. 22, 2022).